Photo-crosslinkable PEG-Based Microribbons for Forming 3D Macroporous Scaffolds with Decoupled Niche Properties

*Li-Hsin Han, Xinming Tong, and Fan Yang**

The extracellular matrix (ECM) is a 3D multi-factorial microenvironment, and cell fate is dictated by complex, interactive niche signals that include biochemical, mechanical, and topographical cues.[1–3] To promote desirable cellular processes and tissue formation, extensive attempts have been made to develop biomaterials as an artificial niche that mimics the biochemical and mechanical properties of the ECM.[4–10] Recent studies have shown that scaffold topographical cues, such as macroporosity and surface curvature, can also be engineered to promote cell proliferation, vascularization, and tissue formation.[11–16] Given that the cell and ECM often interact in a complex and non-intuitive manner, macroporous scaffolds that possess decoupled niche properties are highly desirable for possibly elucidating how interactive niche signals regulate cell fates and tissue formation. Towards this goal, we report the development of 3D scaffolds with decoupled biochemical, mechanical, and topographical properties using microribbon-like, poly(ethylene glycol) (PEG)-based hydrogels, which can further inter-crosslink to form 3D macroporous scaffolds that allow the direct encapsulation of cells.

A few recent studies have attempted to create hydrogel-based scaffolds with decoupled biochemical and mechanical properties;[5–8] however, these platforms generally have limited tunability with regards to the topographical properties. Furthermore, current methods to introduce topographical cues into 3D scaffolds often involve non-physiological fabrication conditions, such as stereolithography, electrospinning, lyophilizing, and salt-leaching.[17–20] As a result, cells can only be seeded after scaffold fabrication, which often results in non-uniform cell distribution and tissue formation.[19,21–23] Recently, we reported the development of a cell-friendly process for fabricating macroporous scaffolds using gelatin-based, microribbon-like hydrogels as building blocks, which can further crosslink together to form 3D scaffolds with tunable macroporosity.[13] The resulting scaffold supported rapid cell proliferation of human-adipose-derived stromal cells in three dimensions, and it demonstrated great mechanical flexibility when subject to cyclic compression. One limitation that remains with the gelatin-based microribbon scaffold is that as a collagen-derived natural biomaterial, it is subject to potential batch-to-batch variability, and it does not allow decoupled tunability of the biochemical and mechanical cues.

As such, the goal of this study is to develop synthetic polymer-based microribbons as building blocks for forming 3D macroporous scaffolds with independently tunable biochemical, mechanical, and topographical cues that support direct cell encapsulation. We have chosen eight-arm PEG with different functional end-groups for the base materials because of its biological inertness and amenability to chemical modification.[24] We first produced PEG hydrogels with microribbon-like structures by wet-spinning eight-arm PEG structures with varying end-group chemistry (**Figure 1**A). The stiffness of the wet-spun microribbons can be tuned by varying the ratios of the PEG components with varying end-group chemistry. The biochemical cue on microribbons was subsequently introduced by covalently linking biochemical ligands of choice; this allows for spatial patterning of multiple bioactive ligands in three dimensions so as to mimic tissue zonal organization. As a proof-of-principle study, we encapsulated human-adipose-derived stromal cells (hADSCs) in 3D scaffolds with decoupled niche properties; the scaffolds were formed using PEG-based microribbons. A total of eight groups were examined with independently tunable biochemical cue (peptide Cys-Arg-Gly-Asp-Ser (CRGDS) versus (vs.) cysteine), stiffness (6 kPa vs. 80 kPa), and macroporosity (5% vs. 3.8% (w/w)). Outcomes were examined by considering cell morphology and cell proliferation using confocal microscopy imaging and biochemical assays.

To synthesize PEG-based microribbons with tunable biochemical and mechanical properties, we selected eight-arm PEG with *N*-hydroxysuccinimide (NHS) end-groups (PEG-$(NHS)_8$; molecular weight, MW ≈ 10 kDa) as the starting materials. To tune the microribbon stiffness, half of the NHS end-groups on eight-arm PEG were substituted by either hydroxyl groups (–OH) or methacrylate (–MA) moieties to produce PEG-$(NHS)_4$-$(OH)_4$ and PEG-$(NHS)_4$-$(MA)_4$, respectively (Figure 1B,C). By varying the ratio of PEG-$(NHS)_4$-$(OH)_4$ and PEG-$(NHS)_4$-$(MA)_4$ in the precursor solution for wet-spinning, we can obtain microribbons with different stiffnesses. Specifically, increasing the ratio of PEG-$(NHS)_4$-$(MA)_4$ increases the stiffness of the resulting microribbons because the methacrylate end-groups (MA) allows further crosslinking of the microribbons during the later photo-polymerization process for 3D scaffold formation. The wet-spun PEG microribbons are bio-inert, which provides a blank slate for biochemical modification. To introduce biochemical ligands onto the microribbon

Dr. L.-H. Han, Dr. X. M. Tong, Prof. F. Yang
Department of Orthopaedic Surgery
Stanford University
Stanford, CA, 94305, USA
E-mail: fanyang@stanford.edu
Prof. F. Yang
Department of Bioengineering
Stanford University
Stanford, CA, 94305, USA

DOI: 10.1002/adma.201304805

© 2013 WILEY-VCH Verlag GmbH & Co. KGaA, Weinheim

ADVANCED MATERIALS
www.advmat.de

www.MaterialsViews.com

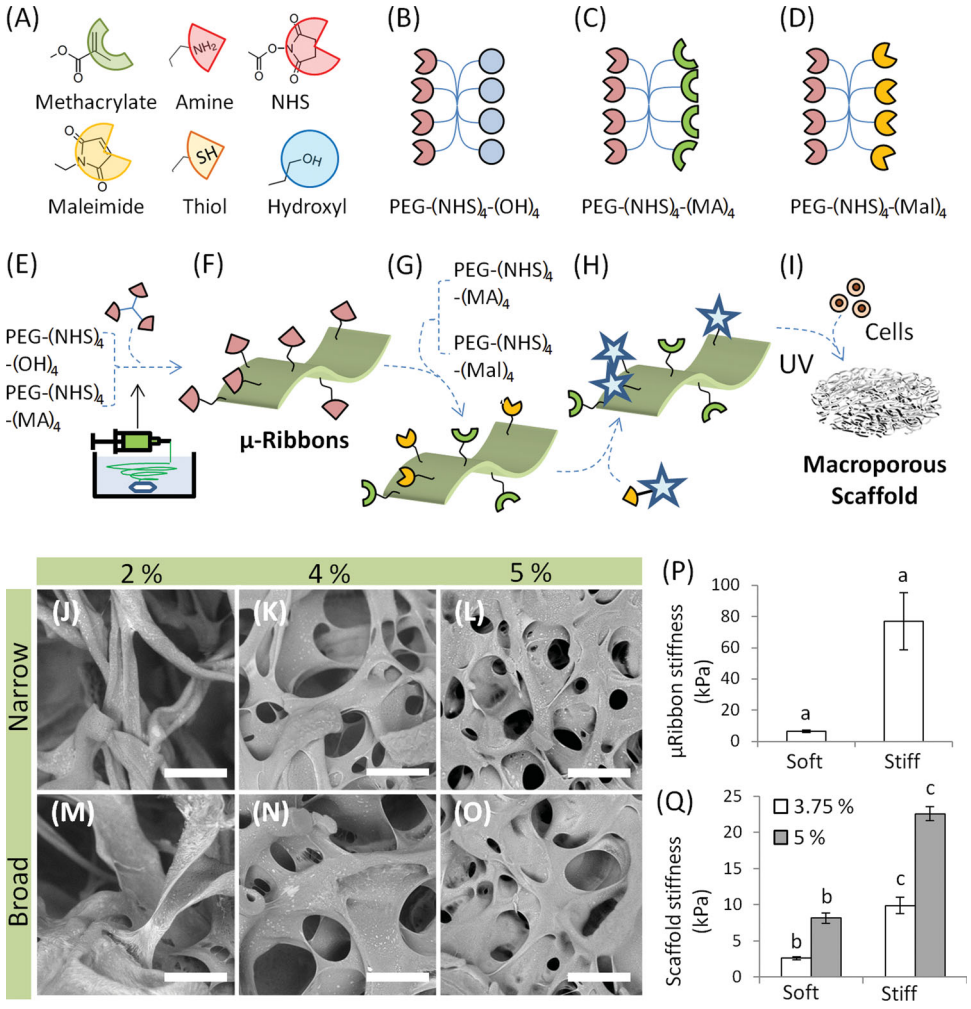

Figure 1. A–I) Schematics and material compositions for fabricating PEG-based, microribbon-like hydrogels, which can further crosslink to form 3D macroporous scaffolds in the presence of cells. A) Symbols representing the different end-groups used on the eight-arm PEG. B,C) Eight-arm PEG precursors (PEG-$(NHS)_4$-$(OH)_4$ and PEG-$(NHS)_4$-$(MA)_4$) were used for fabricating microribbons with tunable stiffness. D) PEG-$(NHS)_4$-$(Mal)_4$ was used for incorporating thiolated biochemical ligands. Schematics showing E,F) the fabrication of microribbons with tunable stiffness by wet-spinning eight-arm PEG precursors with varying ratios, which were subsequently crosslinked via amine–(NHS) reaction; G,H) the introduction of functional groups to the surface of the PEG microribbons so as to allow incorporation of thiolated biochemical ligands (via PEG-$(NHS)_4$-$(Mal)_4$ coating) and further photo-crosslinking among the microribbons (via additional PEG-$(NHS)_4$-$(MA)_4$ coating); and H,I) the direct encapsulation of cells in microribbon-based scaffolds upon photo-crosslinking. J–O) SEM images of internal morphology of the 3D microribbon-based scaffolds formed using varying microribbon densities (2%, 4%, 5%) and microribbon widths (scale bars: 200 μm). P) Tuning the microscopic stiffness of individual microribbon by varying the ratio of PEG-$(NHS)_4$-$(MA)_4$ vs. PEG-$(NHS)_4$-$(OH)_4$ (0:1→ soft, 1:0→ stiff). Q) Tuning the macroscopic stiffness of microribbon-based scaffolds by varying microribbon density. Groups in (P,Q) sharing the same letters are statistically different from each other ($p < 0.005$).

surface, the microribbons of varying stiffness can be subsequently coated with PEG-$(NHS)_4$-$(Mal)_4$ precursor, which was synthesized by substituting half of the NHS end-groups of PEG-$(NHS)_8$ with maleimide (Mal) end-groups (Figure 1D). We chose the maleimide cross-linking chemistry for incorporating biochemical cues because of its mild and rapid reaction, demonstrated cell compatibility, and the ease with which thiolated proteins or peptides can be incorporated through thiol–ene coupling.[25] The wet-spinning process to fabricate PEG-based microribbons is outlined in Figure 1E,F. The PEG precursors (PEG-$(NHS)_4$-$(OH)_4$ and PEG-$(NHS)_4$-$(MA)_4$) were dissolved in acetonitrile and mixed at varying ratio to control the stiffness of the resulting microribbons, and then injected from a syringe pump into a tris(2-aminoethyl) amine (TAEA) bath under constant stirring (125 rpm) (Figure 1E). Under the shear force of the stirring flow, the TAEA crosslinked the PEG precursor solution producing microribbon-shaped hydrogels (Figure 1F and the Supporting Information (SI), Video S1). By adjusting the feeding rate of precursors from 2.5 to 5.0 mL/h, the width of the microribbons can be tuned from 50 to 200 μm. The as-spun microribbons were then coated with PEG-$(NHS)_4$-$(Mal)_4$ for biochemical tunability and additional PEG-$(NHS)_4$-$(MA)_4$ to allow inter-crosslinking among microribbons to form 3D macroporous scaffolds (Figure 1G). The as-fabricated PEG-based microribbons were washed with phosphate-buffered saline (PBS), concentrated by centrifugation,

© 2013 WILEY-VCH Verlag GmbH & Co. KGaA, Weinheim
Adv. Mater. 2013,
DOI: 10.1002/adma.201304805

and kept hydrated in PBS. To quantify microribbon density, a small portion of the concentrated microribbons were collected, measured for wet-weight, freeze-dried, and finally measured for dry-weight. When constructing scaffolds, microribbon density in the macroporous scaffolds was defined as dry-weight over wet-weight (w/w). For direct cell encapsulation, PEG-based microribbons were suspended in PBS at the desired microribbon density, mixed with cells at the desired cell density, and photo-crosslinked (365 nm, 2.5 mW/cm^2, 4 min) into cell-laden, macroporous scaffolds in the presence of the photo-initiator phenyl-2,4,6-trimethylbenzoyl-phosphinate (LAP; Figure 1I).[26] Scanning electron microscopy (SEM) imaging showed that the crosslinked PEG-microribbons resembled a "highway system" with interconnected macroporosity throughout the whole scaffold (Figure 1J–O). The level of macroporosity can be tuned by varying the density or width of the PEG microribbons. For example, increasing the microribbon density from 2% to 5% (w/w) decreased the sizes of macropores from 300–500 μm to 50–100 μm (Figure 1J vs. 1L). Similar results may also be achieved by increasing the width of microribbon blocks from 50–100 μm to 100–200 μm. Macroporosity also affects the average surface curvatures for cell adhesion, which may influence cell fate by modulating cytoskeleton tension in 3D.[14,15,27]

Increasing evidence has highlighted the importance of matrix stiffness in dictating cell fates such as stem-cell differentiation and self-renewal.[28–30] One advantage of our microribbon-based scaffold design is the ability to decouple microscopic stiffness that cells sense from the macroscopic stiffness of the bulk scaffold. Specifically, the microscopic matrix stiffness that cells sense is dictated by the stiffness of each individual microribbon, whereas the macroscopic stiffness of the bulk scaffold can be controlled by varying the density of microribbon building blocks. In our design, we can tune the stiffness of individual PEG-based microribbons by varying the ratio between PEG-$(NHS)_4$-$(MA)_4$ and PEG-$(NHS)_4$-$(OH)_4$ during wet spinning. Specifically, by increasing the proportion of PEG-$(NHS)_4$-$(MA)_4$ from 0% to 100%, we increased the stiffness of PEG-microribbons from 6.4 ± 0.7 to 76.9 ± 18.3 kPa (Figure 1P), a range that has been shown to induce mesenchymal stem cell (MSC) differentiation toward multiple lineages such as muscles, cartilage, and bones.[29] The macroscopic mechanical properties of the crosslinked microribbon scaffold can be tuned by varying the stiffness and density of microribbon building blocks. Increasing the density of soft (~6 kPa) microribbons from 3.75% to 5% (w/w) increased the scaffold stiffness from 2.6 ± 0.2 to 8.2 ± 0.7 kPa, and increasing the density of stiff (~80 kPa) microribbons from 3.75 to 5% (w/w) increased the scaffold stiffness from 9.9 ± 1.1 to 22.6 ± 1.0 kPa (Figure 1Q).

The ability of scaffold to sustain compression is an important aspect for engineering load-bearing tissues such as cartilage and bone, but it is often difficult to achieve using conventional hydrogels. We specifically chose the geometry of microribbons, which resembles thin cantilever beams that transmit mechanical loading easily by bending deformation.[31] Microribbons are inherently flexible due to the low area moment of inertia rendered by the microribbon morphology:[31]

$$J_{ww} = \frac{A^2}{12}\left(\frac{t}{w}\right) \quad (1)$$

where A represents the microribbon's cross-sectional area, w and t the width and thickness of the microribbons, respectively, and J_{ww} the microribbons' area moment of inertia, which quantifies the resistance to the bending deformation of the microribbon. The flat cross-section of microribbons produced small J_{ww} values, which renders high flexibility of the resulting microribbons and scaffolds. We have reported recently that 3D scaffolds formed using gelatin microribbons demonstrated superior flexibility and mechanical stability compared to scaffolds formed using gelatin microfibers with round cross-sections.[13] We performed mechanical testing on scaffolds formed using the PEG-based microribbons, and showed the resulting scaffolds could sustain 40%, 1-Hz cyclic compression without failing using 5% (w/w) stiff PEG-microribbon modules (SI: Video S2).

The biochemical cue that cells would sense in a microribbon-based scaffold is determined by the surface chemistry. To examine the efficacy of biochemical ligand incorporation, PEG-based microribbons consisting of the "stiff" precursor (PEG-$(NHS)_4$-$(MA)_4$) and a maleimide coating were treated with cell-adhesive peptide CRGDS, in which the cysteine (Cys) end-group can be covalently linked with maleimide via thiol–ene addition. Microribbons coated with Cys were included as a control. We then seeded hADSCs on the top of the resulting sheets of the crosslinked microribbon-scaffolds, and examined cell morphology using fluorescence staining of microtubules and actin filaments. We observed extensive hADSC spreading on the CRGDS-treated microribbons (**Figure 2**A), whereas cells remained spherical and formed small cell clusters on the Cys-treated microribbons (Figure 2B). Such a difference in cell spreading can lead to very distinct cell behaviors. Recent studies have shown that the distribution of the actin cytoskeleton and associated cell morphology affect many cellular processes, including cell proliferation and differentiation,[32,33] which can also modulate tissue formation. Histogram analyses of cell area (number of data, $n > 300$) confirmed that the CRGDS-treated microribbons significantly enhanced cell spreading in comparison with Cys-treated microribbons (Figure 2C). These results confirm that our method allows effective incorporation of biochemical cues onto the microribbon surface while retaining biological activity. As most tissue regeneration requires the synergy of multiple types of biochemical ligands, our PEG-based microribbons possessed the biochemical tunability to incorporate a variety of biomolecules including peptides, proteins, and glycoaminoglycans to promote desirable tissue formation. We also assessed the effects of varying microribbon stiffness on cell morphology by plating hADSCs on scaffolds fabricated from either soft (~6 kPa) or stiff (~80 kPa) microribbons functionalized with CRGDS. Immunostaining of actin filaments (green) and α-tubulin (red) showed that both groups supported cell adhesion and spreading by day 3, with more extensive cell-spreading observed on stiff microribbons in comparison with the soft microribbons (Figure 2D–F).

We then explored the potential to spatially pattern different biochemical cues in microribbon-based scaffolds. This would be particularly useful for recreating zonal organization for tissue regeneration or for studying cell responses to spatially patterned biochemical cues. As a proof-of-principle study, we used fluorescein (green) or rhodamine (red)-labeled fibrinogen

© 2013 WILEY-VCH Verlag GmbH & Co. KGaA, Weinheim

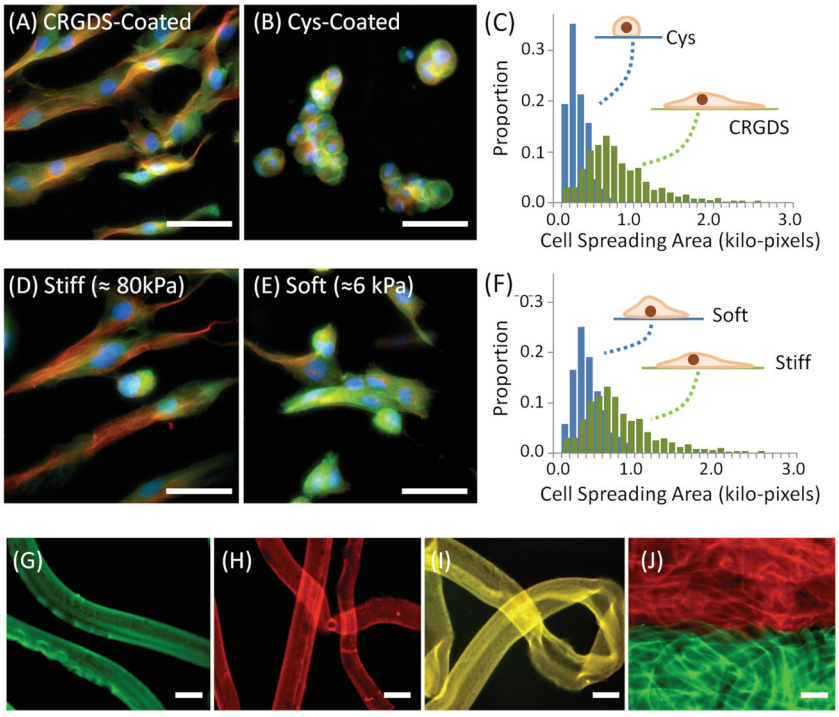

Figure 2. A–F) Effects of changing the biochemical cues and stiffness of the PEG microribbons on the morphology of hADSCs: A,B) hADSCs cultured on CRGDS-coated microribbons (A) or Cys-coated microribbons (B). C) Histogram of cell area showed enhanced cell spreading on CRGDS-coated microribbons compared to that on Cys-coated microribbons. D,E) hADSCs cultured on stiff (D) or soft (E) microribbons. F) Histogram of cell area showed enhanced cell spreading on the stiff microribbon. G–I) Coating microribbons with fluorescein- and rhodamine-labeled fibrinogen at different molar ratios: 1:0 (G), 0:1 (H), and 1:1 (I). J) Spatial patterning of two biochemical cues in bi-layered structures to mimic the layered tissue zonal organization. Scale bars: 50 μm (A,B,D,E); 200 μm (G–J). Green: actin; Red: α-tubulin; Blue: cell nuclei.

as two model biomolecules to visualize the spatial distribution of the biochemical cues in the scaffold. Fluorescence imaging demonstrated that we can present one type of biochemical cue at a time (Figure 2G,H) or co-localizing two biochemical ligands simultaneously (Figure 2I), which would be useful in scenarios where co-localization of multiple biochemical ligands are needed to activate desirable cellular responses. Microribbons with distinctive biochemical cues can be spatially patterned (Figure 2J) to mimic the zonal organization of native tissues, such as the laminar organization of cartilage.[34] While we demonstrated a bi-layered patterned structure as an example, it is easy to adapt the platform to create more complex patterns that mimics zonal organization of specific tissue types.

Macroporosity in tissue engineering scaffolds is desirable and supports tissue regeneration by facilitating nutrient diffusion, cell proliferation, ECM production, and faster blood-vessel ingrowth.[11] To demonstrate the effects of tuning macroporosity in our microribbon-based scaffolds on cellular response, hADSC were encapsulated in RGD-functionalized (arginyl–glycyl–aspartic acid), microribbon-based scaffolds with two different microribbon densities (3.8% or 5.0% (w/w)) (**Figure 3**A–D). Increasing microribbon density from 3.8% to 5% (w/w) resulted in a decrease in the size of macropores in the scaffolds. Confocal microscopy showed that the hADSCs cultured within larger macropores exhibited cell spreading mostly on individual microribbons, which is more comparable to a 2D culture (Figure 3A, B). In contrast, hADSCs cultured within smaller macropores formed contacts with multiple microribbons at the same time (Figure 3C,D), which resembled a 3D culture and demonstrated more direct cell–cell contacts (animated confocal images of hADSCs-laden scaffolds with microribbon densities of 3.8% or 5.0% are provided in the SI: Videos S3 and S4, respectively).

One unique advantage of the PEG-based, microribbon-like hydrogels is that they allow independently tunable niche properties of the resulting macroporous scaffolds. We have recently reported gelatin-based microribbons for fabricating macroporous scaffolds with enhanced flexibility.[13] One major limitation of the gelatin-based microribbons is their limited tunability in biochemical and mechanical cues. Like other naturally derived materials, changes in the concentration of gelatin would simultaneously induce changes in the biochemical, mechanical and degradation properties of the resulting microribbons. In contrast, the PEG-based microribbons reported herein are intended to fill a critical void in the available biomaterials platform with independently tunable niche cues. Such a biomaterials platform would provide useful tools to enable analyses of how complex niche cues interplay to influence cell fates and tissue formation. As a proof-of-principle study, hADSCs were encapsulated in eight groups of microribbons-based scaffolds with varying biochemical cues (CRGDS vs. Cys), microribbon stiffness (6 kPa vs. 80 kPa), and macroporosity (by varying microribbon densities; 3.8% vs. 5.0% w/w) (Figure 3E). Cell proliferation inside different scaffolds was quantified on day 6 using a WST-8 assay (Figure 3F). As expected, all scaffolds coated with CRGDS resulted in higher cell proliferation by 2–9-fold compared to their respective control groups coated with Cys. The highest cell proliferation was observed in RGD-containing, softer-microribbon-based scaffolds (6 kPa) with smaller macropores (5%). At the higher microribbon density (5%, CRGDS), soft microribbons resulted in 126% more cell proliferation compared to stiff microribbons (80 kPa; $p < 0.001$). This might be attributed to the larger surface area for cell adhesion and proliferation in scaffolds with higher microribbon density. Interestingly, varying microribbon stiffness did not markedly change cell proliferation in microribbon-based scaffolds with larger macroporosity (3.8%), suggesting that the interactions of multi-factorial niche signals are non-linear and cannot be predicted by optimizing individual niche cues sequentially.

Another advantage of the PEG-based microribbons is the ease with which to customize microribbon stability and degradability so as to accommodate the desirable tissue formation. This can be achieved by introducing hydrolytically or enzymatically

© 2013 WILEY-VCH Verlag GmbH & Co. KGaA, Weinheim
Adv. Mater. **2013**,
DOI: 10.1002/adma.201304805

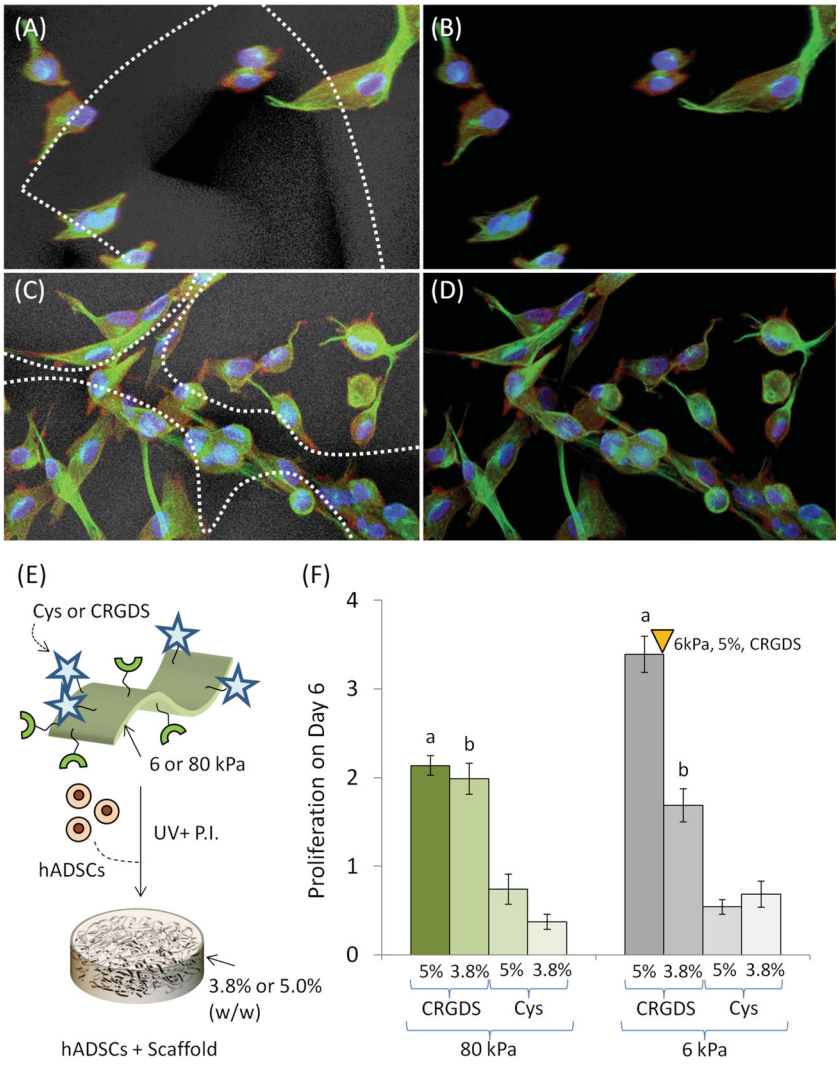

Figure 3. Cell spreading and proliferation in microribbon-based scaffolds with tunable biochemical, mechanical, and topographical cues: A–D) Morphology of hADSCs in scaffolds with large macropores (~300 μm; A,B) or scaffolds with smaller pores (<100 μm; C,D). Images were reconstructed from confocal microscopy images with (A,C) or without (B,D) microribbons. E) Encapsulation of hADSCs among microribbons with independently tunable stiffness (6 kPa vs. 80 kPa), biochemical cues (Cys vs. CRGDS), and microribbon densities (3.8% vs. 5.0%) (w/w). F) Cell proliferation in 8 groups of microribbon-based scaffolds with varying compositions and cell proliferation was normalized to day 0. Groups in (F) sharing the same letters are statistically different from each other (a: $p < 0.0001$, b: $p < 0.05$). Green: α-tubulin; Red: actin; Blue: cell nuclei.

degradable sequences into the PEG backbone. Compared to the previously reported gelatin microribbon platform,[13] the PEG-based microribbons reported here allow greater tunability in ribbon properties, and may be used for engineering a broad range of tissue types.

Unlike other topographical structures commonly used in scaffold design such as nanofibers, our PEG-based microribbons provide unique advantages as building blocks for fabricating a 3D cell niche. First, these microribbons are intercrosslinkable, and support direct cell encapsulation while simultaneously forming macroporous scaffolds. In contrast, conventional nanofibrous scaffolds require pre-fabrication; cells are seeded post-fabrication, and often lack homogeneity and macroporosity. Second, the PEG-based microribbons allow independently tunable niche properties (i.e., stiffness, biochemical ligands, macroporosity), which is designed specifically to facilitate mechanistic studies of cell–niche interactions. Third, we have chosen the microribbon morphology (flat cross-section) to absorb additional force when subject to compression, which leads to a scaffold with higher flexibility compared to the conventional fibrous scaffolds (round cross-section).

In summary, here we report the design and synthesis of PEG-based, crosslinkable microribbons as building blocks for fabricating a cell-laden, macroporous scaffold with independently tunable niche properties including biochemical, mechanical, and topographical cues. Such biomaterial platforms could provide a valuable tool for facilitating the analyses of how the interaction of multi-factorial niche signaling influences cell fate in 3D. Meanwhile, it may also be used to promote desirable cellular processs and tissue formation through fine tuning of the scaffold cues to identify optimal scaffold compositions. The unique geometry of microribbons renders the resulting scaffold with flexibility to absorb cyclic stress, which would be particularly useful for engineering tissues types where flexibility is desirable, such as musculoskeletal tissues or cardiovascular tissues. Finally, our platform also supports facile spatial patterning of biochemical cues in 3D, which can facilitate recreating the zonal organization observed in many tissue types.

Supporting Information

Supporting Information, including experimental protocols, is available from the Wiley Online Library or from the author.

Acknowledgements

This work was supported by the McCormick Faculty Award at Stanford University, a Basil O'Connor Starter Scholar Research Award from the March of Dimes Foundation, a Stanford Bio-X Interdisciplinary Initiatives grant, and the California Institute for Regenerative Medicine (Grant #TR3–05569). We thank Anthony Behn for his technical assistance in mechanical testing.

Received: September 25, 2013
Revised: October 28, 2013
Published online:

© 2013 WILEY-VCH Verlag GmbH & Co. KGaA, Weinheim

[1] D. T. Scadden, *Nature* **2006**, *441*, 1075–1079.
[2] G. H. Underhill, S. N. Bhatia, *Curr. Opin. Chem. Biol.* **2007**, *11*, 357–366.
[3] J. A. Burdick, G. Vunjak-Novakovic, *Tissue Eng. A* **2009**, *15*, 205–219.
[4] E. Cukierman, R. Pankov, D. R. Stevens, K. M. Yamada, *Science* **2001**, *294*, 1708–1712.
[5] C. A. DeForest, B. D. Polizzotti, K. S. Anseth, *Nat. Mater.* **2009**, *8*, 659–664.
[6] C. A. Deforest, E. A. Sims, K. S. Anseth, *Chem. Mater.* **2010**, *22*, 4783–4790.
[7] M. Nii, J. H. Lai, M. Keeney, L. H. Han, A. Behn, G. Imanbayev, F. Yang, *Acta Biomater.* **2013**, *9*, 5475–5483.
[8] D. S. Benoit, M. P. Schwartz, A. R. Durney, K. S. Anseth, *Nat. Mater.* **2008**, *7*, 816–823.
[9] M. P. Lutolf, J. A. Hubbell, *Nat. Biotechnol.* **2005**, *23*, 47–55.
[10] E. S. Place, N. D. Evans, M. M. Stevens, *Nat. Mater.* **2009**, *8*, 457–470.
[11] S. J. Hollister, *Nat. Mater.* **2005**, *4*, 518–524.
[12] L. H. Han, J. H. Lai, S. Yu, F. Yang, *Biomaterials* **2013**, *34*, 4251–4258.
[13] L.-H. Han, S. Yu, T. Wang, A. W. Behn, F. Yang, *Adv. Funct. Mater.* **2013**, *23*, 346–358.
[14] M. Rumpler, A. Woesz, J. W. C. Dunlop, D. J. T. van, P. Fratzl, *J. R. Soc. Interface* **2008**, *5*, 1173–1180.
[15] J. A. Sanz-Herrera, P. Moreo, J. M. Garcia-Aznar, M. Doblare, *Biomaterials* **2009**, *30*, 6674–6686.
[16] M. Jamal, N. Bassik, J.-H. Cho, C. L. Randall, D. H. Gracias, *Biomaterials* **2010**, *31*, 1683–1690.
[17] D. Y. Fozdar, P. Soman, J. W. Lee, L. H. Han, S. Chen, *Adv. Funct. Mater.* **2011**, *21*, 2712–2720.
[18] J. Rnjak-Kovacina, S. G. Wise, Z. Li, P. K. M. Maitz, C. J. Young, Y. Wang, A. S. Weiss, *Biomaterials* **2011**, *32*, 6729–6736.
[19] J. Xiao, H. Duan, Z. Liu, Z. Wu, Y. Lan, W. Zhang, C. Li, F. Chen, Q. Zhou, X. Wang, J. Huang, Z. Wang, *Biomaterials* **2011**, *32*, 6962–6971.
[20] M. J. Mondrinos, R. Dembzynski, L. Lu, V. K. Byrapogu, D. M. Wootton, P. I. Lelkes, J. Zhou, *Biomaterials* **2006**, *27*, 4399–4408.
[21] S. Y. Chew, R. Mi, A. Hoke, K. W. Leong, *Adv. Funct. Mater.* **2007**, *17*, 1288–1296.
[22] Y. Hong, J. Guan, K. L. Fujimoto, R. Hashizume, A. L. Pelinescu, W. R. Wagner, *Biomaterials* **2010**, *31*, 4249–4258.
[23] A. P. Zhang, X. Qu, P. Soman, K. C. Hribar, J. W. Lee, S. Chen, S. He, *Adv. Mater.* **2012**, *24*, 4266–4270.
[24] J. Zhu, *Biomaterials* **2010**, *31*, 4639–4656.
[25] E. A. Phelps, N. O. Enemchukwu, V. F. Fiore, J. C. Sy, N. Murthy, T. A. Sulchek, T. H. Barker, A. J. Garcia, *Adv. Mater.* **2012**, *24*, 64–70.
[26] B. D. Fairbanks, M. P. Schwartz, C. N. Bowman, K. S. Anseth, *Biomaterials* **2009**, *30*, 6702–6707.
[27] S. Nuernberger, N. Cyran, C. Albrecht, H. Redl, V. Vecsei, S. Marlovits, *Biomaterials* **2010**, *32*, 1032–1040.
[28] D. E. Discher, P. Janmey, Y. L. Wang, *Science* **2005**, *310*, 1139–1143.
[29] S. S. Adam , J. Engler, H. L. Sweeney, D. E. Discher, *Cell* **2006**, *126*, 677–689.
[30] P. M. Gilbert, K. L. Havenstrite, K. E. Magnusson, A. Sacco, N. A. Leonardi, P. Kraft, N. K. Nguyen, S. Thrun, M. P. Lutolf, H. M. Blau, *Science* **2010**, *329*, 1078–1081.
[31] W. D. Callister, *Materials Science And Engineering: An Introduction*, 7th ed., John Wiley & Sons, New York **2007**.
[32] P. de Lanerolle, L. Serebryannyy, *Nat. Cell Biol.* **2011**, *13*, 1282–1288.
[33] M. Versaevel, T. Grevesse, S. Gabriele, *Nat. Commun.* **2012**, *3*, 671.
[34] T. A. Einhorn, R. J. O'Keefe, J. A. Buckwalter, *Orthopaedic Basic Science: Foundations of Clinical Practice*, 3rd ed., American Association of Orthopedic Surgeons, Rosemount, *IL* **2007**.

© 2013 WILEY-VCH Verlag GmbH & Co. KGaA, Weinheim
Adv. Mater. **2013**,
DOI: 10.1002/adma.201304805